Elastic wave-equation migration for isotropic and HTI media

Richard A. Bale and Gary F. Margrave, CREWES, University of Calgary.

2005 CSEG National Convention

Abstract

Prestack wave-equation migration of isotropic or anisotropic elastic seismic data is described as vector wavefield extrapolation, plus an imaging condition for combinations of shot and receiver wave-modes. For azimuthally anisotropic data, the effect is to combine the (normally separate) steps of shear-wave splitting correction and migration into a single migration step. This enables a more accurate correction of the shear waves based upon the local propagation direction. The algorithm is extended to laterally varying medium with two different forms of generalized phase shift operators. The first, which we call "phase shift plus adaptive windowing" (PSPAW), is appropriate for anisotropic media described by several parameters. The second, based on conventional phase shift plus interpolation (PSPI), has been formulated for isotropic media, but is computationally intractable for general anisotropic media.

The PSPAW algorithm has been applied to numerically modeled data, for a model which contains a faulted HTI. The isotropic PSPI algorithm has been applied to a new elastic version of the well-known Marmousi model, to test the ability of this algorithm with highly variable media. The preliminary results are encouraging, especially for the shallow imaging of the converted wave data.

Introduction

Wavefield extrapolation is at the heart of the class of migration algorithms commonly referred to as wave-equation migration. A wavefield extrapolator, as used in such migration schemes, generates the wavefield at depth $z + \Delta z$ from the wavefield at depth z, given the medium parameters over the depth interval. For medium parameters that vary only with depth, this leads to a phase-shift algorithm. In realistic cases where the medium varies laterally, a standard approach is to assume a solution of the same form, but with velocity as a function of lateral position. This results in several alternative algorithms, such as the generalized phase shift plus interpolation (GPSPI) algorithm, and the nonstationary phase shift (NSPS) algorithm (Margrave and Ferguson, 1999). The GPSPI algorithm is an analytic formulation of Gazdag and Sguazzero's (1984) PSPI algorithm; in GPSPI an extrapolation operator is designed uniquely for each output point.

The above remarks apply to scalar-wave equation extrapolators. Strictly speaking, these are only appropriate for migration in acoustic media. Nevertheless, they have been highly successful when applied to the migration of P-wave data obtained from conventional seismic surveys. However, there are disadvantages in using a scalar-wave equation for extrapolating elastic-wave data. First, the scalar-wave approach assumes that each wave-mode can be handled independently of the others, yet conversion between modes is commonplace. Second, scalar wavefield extrapolation cannot keep track of changes in polarization that occur during wave propagation. Finally, it is difficult to account fully for effects of anisotropy, such as shear-wave splitting, using a scalar extrapolator. For these reasons it is sometimes preferable to approach elastic wavefield extrapolation from a vector wave equation standpoint.

Imaging elastic data in the presence of azimuthal anisotropy, for example in vertically fractured reservoirs, is complicated by shear-wave splitting. Conventionally, this is tackled by horizontal component rotations to isolate the fast (S1) and slow (S2) shear waves. The separate S1 and S2 data may then be separately migrated, or simply recombined into a single shear-wave dataset after a vertical shift to align them before migration. There are some approximations implicit in this approach, which is essentially based on vertical propagation theory. For example, the rotation step assumes that the polarizations are orthogonal and lie within the horizontal plane. In fact, for shear waves arriving at oblique angles the polarizations cannot be correctly handled by horizontal rotation, since they are not orthogonal within that plane. Furthermore, the shear-wave velocities for azimuthally anisotropic media are dependent on propagation direction. The "fast" and "slow" shear-wave velocities may even cross over at larger phase angles. There is no single static shift that will correctly align the two shear waves for all angles. To overcome these limitations, the shear-wave rotation and shift operators both should depend upon phase angle. The central idea of this paper is to incorporate the correction for shear-wave splitting within the wavefield extrapolation. The shear-wave splitting correction and the migration are thus combined, not treated as two separate problems.

In this paper, two alternative algorithms for elastic extrapolation are considered. The first makes use of adaptive windowing. This is referred to as PSPAW (phase shift plus adaptive windowing), an elastic extension of the adaptive Gabor (AGPS) method of Grossman et al. (2002). The second is an alternative elastic PSPI extrapolator that is more closely related to the standard PSPI algorithm of Gazdag and Sguazzero (1984). Migration using PSPAW is applicable to either isotropic or HTI media. Migration using the PSPI extrapolator is optimized for isotropic media.

Theory

The theory required for elastic wavefield extrapolation is based on eigen-solutions to the Kelvin-Christoffel equation and the theory of anisotropic propagator matrices (Fryer and Frazer, 1984; 1987). For wave propagation in a 2-D, laterally homogeneous, HTI medium with horizontal slowness $p_x = k_x/\omega$, the elastic extrapolation operator is

$$\mathbf{b}(p_x, z_{n+1}, \omega) = \mathbf{D}_n(p_x) e^{i\omega \mathbf{\Lambda}_n(p_x)(z_{n+1}-z_n)} \mathbf{D}_n^{-1}(p_x) \mathbf{b}(p_x, z_n, \omega), \quad (1)$$

where $\mathbf{b}$ is a vector containing displacement $\mathbf{u}$ and the (scaled) vertical traction $\boldsymbol{\tau}$, given by $\mathbf{b}^T = \begin{pmatrix}\mathbf{u}^T & \boldsymbol{\tau}^T\end{pmatrix}$. The diagonal matrix, $\boldsymbol{\Lambda}_n = diag(q_n^P \quad q_n^{S1} \quad q_n^{S2})$, contains the vertical slownesses for each mode in layer n, between z_n and z_{n+1}. In the HTI case, the slownesses can be analytically determined. The 6-by-3 matrix, $\mathbf{D}_n$, contains the eigenvectors for each mode, qP, qS1 and qS2, which are solutions to the one-way wave equation in layer n.

In words, equation (1) states the following: decompose the displacement-stress wavefield at the top of layer n into the three eigenstates for layer n, which are the elastic modes; propagate each mode using the vertical slowness for that mode; recombine the modes at the bottom of layer n. The vector $\mathbf{b}$ is, by design, continuous in the presence of medium discontinuities between horizontal layers. Therefore, we may proceed using the extrapolated $\mathbf{b}$ as the boundary condition for the next depth step.

We now generalize equation (1) to spatially variable media. The GPSPI form of equation (1) is

$$\mathbf{b}_{GPSPI}(x, z_{n+1}, \omega) = \frac{\omega}{2\pi}\int_{-\infty}^{\infty} \mathbf{D}_n(x, p_x) e^{i\omega\boldsymbol{\Lambda}_n(x,p_x)(z_{n+1}-z_n)} \mathbf{D}_n^{-1}(x, p_x) \mathbf{b}(p_x, z_n, \omega) e^{-i\omega p_x x} dp_x , \qquad (2)$$

where $\mathbf{b}(p_x, z_n, \omega)$ is the Fourier transform of $\mathbf{b}(x, z_n, \omega)$, resampled to p_x. The key difference compared to equation (1) is that $\mathbf{D}_n$ and $\boldsymbol{\Lambda}_n$ now depend on x. Equation (1) is exact, while equation (2) is only a first-order accomodation for lateral inhomogeneity. Regardless of the strength of lateral gradients, equation (2) will only allow mode conversions at the top or bottom of the depth step. The nature of this approximation is in keeping with that made in scalar wave GPSPI, where refraction only occurs at depth boundaries. Nevertheless, scalar GPSPI is regarded as very accurate for depth migration.

Equation (2) as written is expensive to implement. It cannot be performed using an FFT, due to the x dependence. A practical implementation of this equation involves some form of windowing or interpolation. The traditional PSPI approach is to compute several wavefields with reference models (velocities in the scalar case), return each to the spatial domain with inverse FFTs, and interpolate the results. In the case of anisotropic elastic wavefield extrapolation, the traditional approach has a major drawback. The minimum number of parameters required to represent an HTI medium is six: two velocities, three anisotropy parameters, and the orientation of the symmetry axis. If it is assumed that only 5 reference values are selected for each parameter, then the total number of reference operators required is the 6th power of 5, or 15625. This is clearly intractable, unless the dependence on the parameters is somehow decoupled. In general this is not possible. In the special case of isotropy, where there are only 2 parameters, and the parameter dependence is approximately separable, an approach based on standard PSPI *can* be used.

For HTI media, an alternative approach called PSPAW has been devised to avoid this problem. The basic idea is to form spatial windows within which the phase velocity variation is not too large, and the axis of symmetry doesn't vary too much. Since the phase velocity varies with phase angle, the first criterion is tested for several representative angles. The resulting operators are applied in overlapping windows with weights which sum to unity everywhere. Tests indicate this typically produces a manageable number of operators for each shot migration. Details of both PSPAW and elastic PSPI methods are given in Bale and Margrave (2004).

The extrapalation in equation (2) generates decomposed P, S1 and S2 wavemodes. For shot record migration, the extrapolation is used to forward extrapolate the downgoing wavefield from the source and backward extrapolate the upgoing wavefield measured at the receivers. An imaging condition is then applied to extract appropriate combinations of the downgoing and upgoing wavefields. Selected images, such as P-P, P-S1 and P-S2, are produced simultaneously, using a deconvolution imaging condition.

Examples

The PSPAW algorithm has been tested on a simple model, consisting of a faulted HTI layer sandwiched betwee two isotropic layers, and overlying a fourth isotropic layer. The HTI layer has a symmetry axis direction of 45° to the inline direction. The input data were modeled with a 2-D anisotropic pseudospectral modeling code, using a P-wave source and 3-component receivers. The source signature used was a zero phase Ricker wavelet with 15Hz center frequency. The shot spacing was 200m, from 160m to 4960m, and the receiver range is from 565m to 4555m along the surface.

Figure 1 shows the result of elastic migration applied to the HTI dataset. In addition to the P-P image, which is not shown, two separate P-S images are generated, one for the fast (S1) mode and one for the slow (S2) mode. For isotropic layers, the SV mode is assigned to the S2 section. Based upon this convention, the S1 mode only responds to the top and bottom of the HTI layer, and not to any other interfaces – hence the absence of the flat basement reflector on the second image. When the same data is migrated isotropically an erroneous image of this reflector appears on the S1 section. Similarly, the section of the fault which is bounded by isotropic layers on both sides is invisible on the S1 section, because the S1 only responds to HTI perturbations.

The second example is the elastic Marmousi-2 model, which is isotropic but highly heterogeneous. The Marmousi-2 dataset was generated by the Allied Geophysical Laboratory at the University of Houston (Martin et al., 2002). It is based upon the standard acoustic Marmousi model but with several modifications: it has been extended laterally to a total line length of 17 km, with interesting stratigraphic features and hydrocarbon accumulations; it is an elastic model; and finally, it has been submerged under 500m of water. The modelled data are include both OBC and towed streamer data. We have confined our attention to the OBC dataset. The dataset is somewhat more challenging than the conventional acoustic Marmousi, owing to the presence of multi-mode data, long period water multiples, and aliased water bottom diffractions.

The isotropic elastic PSPI version of the migration was used to image this data. Testing on this dataset is ongoing. The results included here are of a preliminary nature. In particular, the central area (figure 2) poses imaging problems which have yet to be fully resolved. The PSPI migrated images for this area, which corresponds to the upper 2km of the original Marmousi model, are shown in

figure 3. The P-P image is promising, whereas the P-S image is less clearly defined. This may be due to difficulty with correctly handling polarity changes in this complex structure with large Vp/Vs changes. In addition, there are very problematic water layer multiples in the data, seen on both P-P and P-S, as well as aliased seabed diffraction noise.

Figure 4 shows the P- and S-wave impedance sections from a shallow part of the model, located to the left of the area shown in figure 2. This area is considerably less structured, and the horizontal scale in figure 4 has been compressed for display. Figure 5 shows the corresponding P-P and P-S migrated images. As seen in figure 5(b), the shallow P-S imaging is remarkable, displaying clear resolution advantages over the equivalent P-P section in figure 5(a). This is anticipated from theory, due to the slower S-wave velocities, but is striking nonetheless. Also of interest are the very different responses to the gas sand at 0.6km depth to the left of the image. The ability of elastic wave data to provide discrimination between lithology and fluid is exhibited clearly in this example.

Conclusions

A wave-equation migration for elastic seismic data has been developed. The migration uses vector wavefield extrapolators and employs one of two alternative interpolation schemes.

The first, PSPAW, is applicable in the presence of anisotropy. It has been implemented specifically for HTI media, such as may be encountered in vertically fractured reservoirs. The algorithm naturally focuses the separate S1 and S2 wavefields associated with shear-wave splitting, a task which isotropic migration cannot achieve. Lateral variations in the velocities, as well as the degree and orientation of the anisotropy, are accommodated using an adaptive windowing approach. The migration has been demonstrated on a model containing a faulted HTI layer.

The second extrapolator is adapted from the conventional PSPI algorithm. This is only applicable to isotropic media, and in this case an approximation is required for the P-wave modes. It is exactly correct for constant V_P/V_S. This algorithm appears to do a reasonable job on the isotropic, but highly variable, Marmousi-II elastic dataset. There are a number of extraneous issues with these data, primarily related to the water layer, which still need attention. There also appears to be room for improvement in imaging the converted waves in the most structural part of the data.

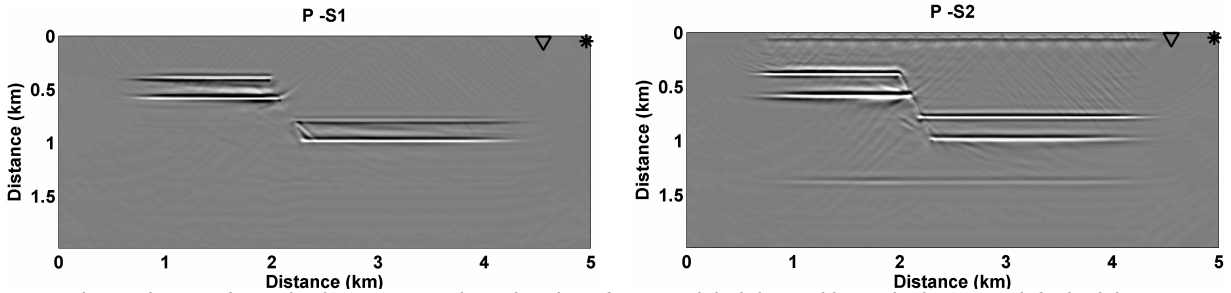

FIG. 1: P-S1 and P-S2 images from elastic wave-equation migration of HTI modeled data, with HTI in the second, faulted, layer. Data migrated with PSPAW method. The flat reflector at 1.4 km depth is a boundary between two isotropic layers. The imaging condition used for isotropic layers assigns SH-waves to S1, and SV-waves to S2. Therefore the reflector appears only on the P-S section, since P does not couple to SH.

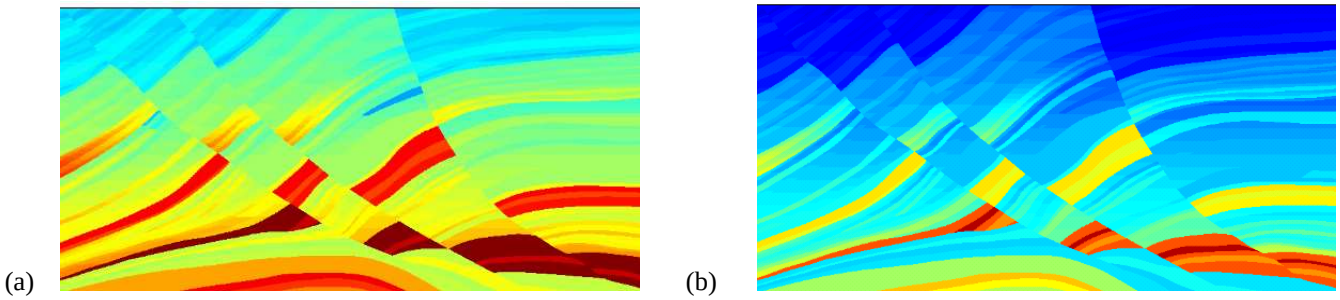

FIG. 2. Marmousi-2 elastic model, showing (a) acoustic (i.e. P-wave) impedance and (b) S-wave impedance. This area corresponds approximately to the original Marmousi acoustic model. The 500m water layer is ommitted.

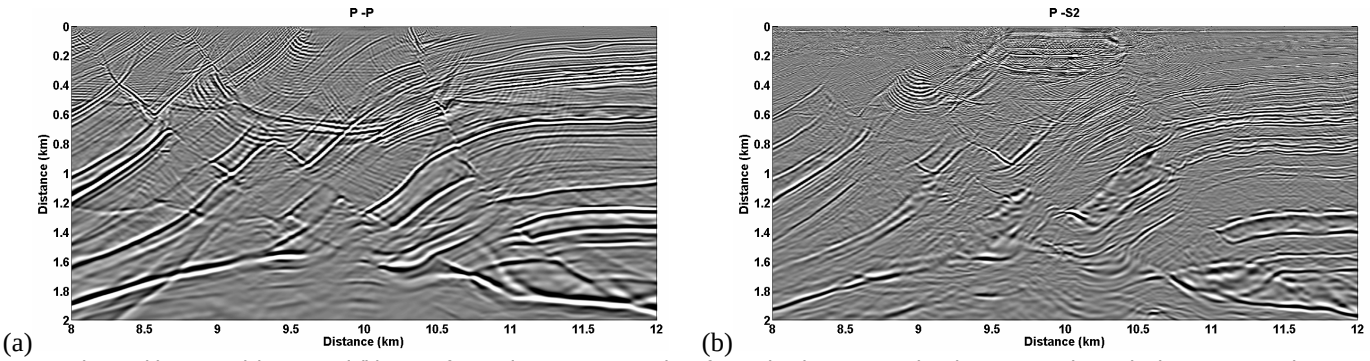

FIG. 3. Migrated images: (a) P-P and (b) P-S of X and Z component data from elastic Marmousi-2 data. Area shown is the same as Figure 2.

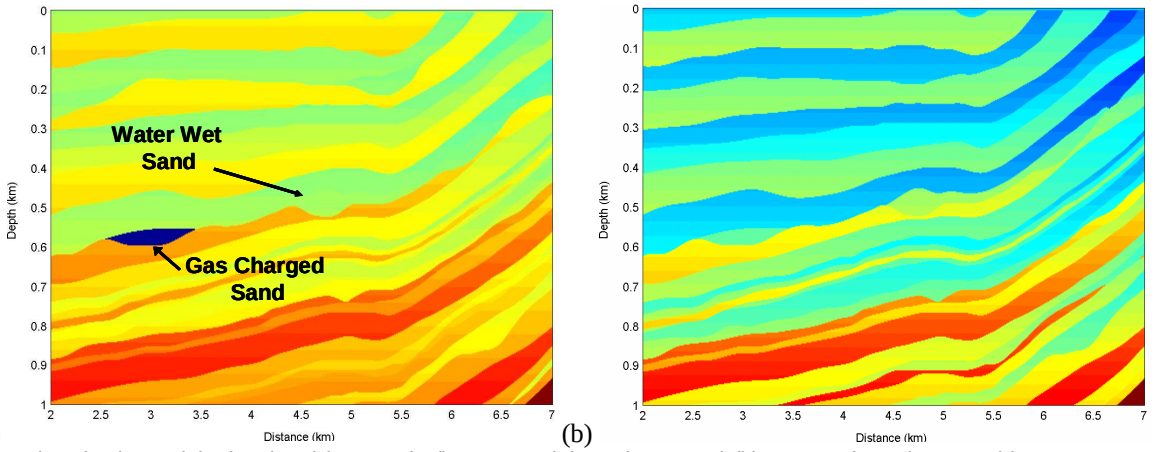

FIG. 4. Marmousi-2 elastic model, showing (a) acoustic (i.e. P-wave) impedance and (b) S-wave impedance. This area corresponds to a shallow section on the left of the main structural area. Note that the horizontal axis has been compressed relative to the vertical, for display purposes. The gas sand is clearly identified by its low P-wave impedance compared to local sediments.

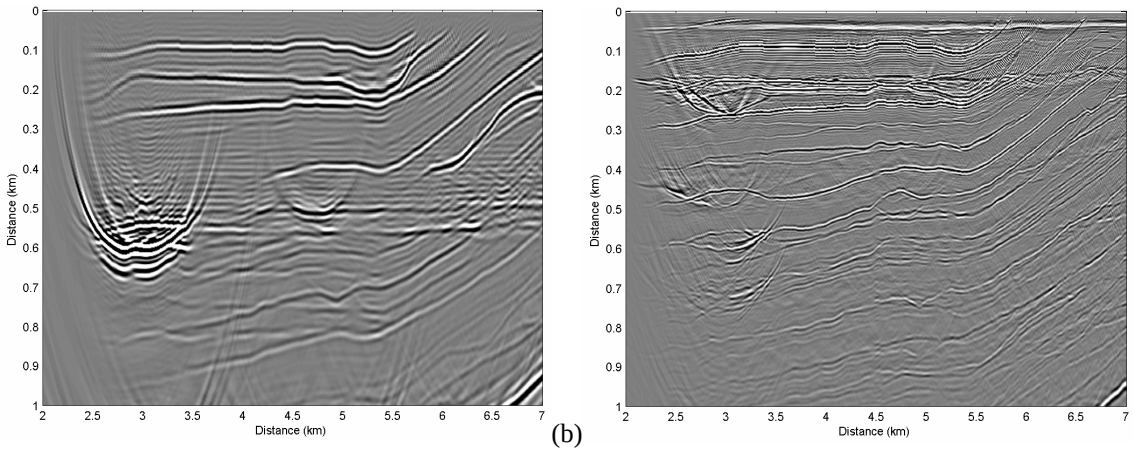

FIG. 5. Migrated images: (a) P-P and (b) P-S of X and Z component data from elastic modeling. Area shown is that of model in Figure 4. Note the superior resolution of the P-S image, and the significantly weaker response to the gas sand. This is an example of fluid-lithology discrimination with elastic waves.

Acknowledgements

The authors gratefully acknowledge the generous support of the sponsors of CREWES and the POTSI (Pseudodifferential Operator Theory and Seismic Imaging) Consortium. The first author is also grateful to Veritas DGC for supporting his ongoing studies.

We also acknowledge the Allied Geophysical Laboratory, at the University of Houston for permission to use the Marmousi II data, and in particular Prof. Robert Wiley and Gary Martin of GX technology for their support and advice regarding the dataset.

We thank Hugh Geiger, Jeff Grossman and Sam Gray for valuable discussions. We especially thank Kevin Hall for his tireless help with the Marmousi-II data and hardware issues.

References

Bale, R.A. and Margrave, G.F., 2004, Elastic wave-equation migration for laterally varying isotropic and HTI media: CREWES Research Report, **16**.

Fryer, G.J. and Frazer, L.N., 1984, Seismic waves in stratified anisotropic media: Geophys. J. Roy. Astr. Soc., **78**, 691-710.

Fryer, G.J. and Frazer, L.N., 1987, Seismic waves in stratified anisotropic media—II. Elastodynamic eigensolutions for some anisotropic systems: Geophys. J. Roy. Astr. Soc., **91**, 73-101.

Gazdag, J. and Sguazerro, P., 1984, Migration of seismic data by phase shift plus interpolation: Geophysics, **49**, 124-131.

Grossman, J.P., Margrave, G.F., and Lamoureux, M.P., 2002, Fast wavefield extrapolation by phase-shift in the nonuniform Gabor domain: CREWES Research Report, **14**.

Margrave, G.F. and Ferguson, R.J., 1999, Wavefield extrapolation by nonstationary phase shift: Geophysics, **64**, 1067-1078.

Martin, G., Larsen, S. and Marfurt, K., 2002, Marmousi-2: an updated model for the investigation of AVO in structurally complex areas, 72nd Ann. Internat. Mtg: Soc. of Expl. Geophys., 1979-1982.